The Effect of Hepatic Radiofrequency Ablation on Stem Cell Trafficking in the Rat Model

Boris Nikolic, MD, MBA, Mostafa Elian, MD, Pawel Mertyna, MD, Sam Yam, PhD, and S. Nahum Goldberg, MD

PURPOSE: To determine whether radiofrequency (RF) ablation causes increased hepatic embryonic stem cell trafficking in the rat liver model.

MATERIALS AND METHODS: Right hepatic lobe RF ablation was performed in rats for 5 minutes at 15 minutes ($n = 2$) and 48 hours ($n = 2$) before administration of rat hepatic embryonic stem cells (rhESCs). Green fluorescent protein–labeled rhESCs were injected intravenously, and all rats were killed 5 days after rhESC injection. Tissue was removed from RF ablation areas and untreated liver, the latter of which served as control. Slides were evaluated with fluorescent microscopy, and software fluorescence count was performed for evaluation of rhESC distribution. Regions of rhESC destination were divided into inner coagulation (zone A), periablational (zone B), and peripheral (zone C) zones. Fluorescence comparison was additionally performed between RF ablation areas and corresponding control tissues of the left hepatic lobe (segment II). Kruskal-Wallis testing was used for evaluations.

RESULTS: Fluorescent pixel count was significantly higher in RF ablation areas than in respective controls: mean at 15 minutes, 10,471 ± 3,830 (SD) versus 1,889 ± 1,427 ($P < .05$); mean at 48 hours, 15,177 ± 7,091 versus 2,868 ± 1,714 ($P < .05$). High-power field samples showed significant distribution differences across zones: zone B, mean, 1,015.4 ± 311; zone A, mean, 17.8 ± 11; and zone C, mean, 141.2 ± 51.4 ($P < .05$).

CONCLUSIONS: RhESCs administered after RF ablation are trafficked to the periablational margin in significantly greater numbers than the remaining liver.

J Vasc Interv Radiol 2009; 20:640–647

Abbreviations: GFP = green fluorescent protein, RF = radiofrequency, rhESC = rat hepatic embryonic stem cell, TBS = Tris-buffered saline

THE ability of stem cells to differentiate into specialized and fully functional parenchymal cells that can be used to improve function or alleviate symptoms related to various disease states has been shown in multiple studies (1–3). It has been demonstrated, for instance, that transplanted stem cells of different origins are able to alleviate pulmonary hypertension in dogs, restore biochemical function of the liver in an animal model of tyrosinemia I, or regenerate axons through chronically denervated peripheral nerves (1–3). Validated methods of stem cell tracking include green fluorescent protein (GFP) stem cell labeling, magnetic resonance imaging of superparamagnetic iron oxide–labeled stem cells, and the use of optical imaging (4–7). To accomplish preferential stem cell deposition to a specific target location, stem cell attraction to an area of acute organ injury has been consistently observed. Stem cell trafficking to the area of acute organ injury has been attributed to the release of certain key cytokines that is associated with acute organ injury (8). For example, acute hepatic injury was found to facilitate stem cell trafficking and engraftment and has classically been inflicted by hepatic injection of carbon tetrachloride or performance of partial hepatectomy (7,9,10). Yet, there are major problems associated with both these techniques: partial hepatectomy subtracts from the overall liver volume and is highly invasive, and carbon tetrachloride injection is difficult to control, is carcinogenic, and has no therapeutic application. At the same time, it must be noted that performance of liver-related locoregional therapy with interventional means, such as radiofrequency (RF) ablation, likewise causes acute focal hepatic injury by inducing an area of coagulation necrosis that stimulates cytokine release, but has much less potential morbidity (11). We therefore hypothesized that performance of RF ablation may also cause increased stem cell trafficking in the liver.

From the Department of Radiology, University of Pennsylvania School of Medicine, 1 Silverstein, 3400 Spruce Street, Philadelphia, PA 19104. Received August 20, 2008; final revision received January 14, 2009; accepted January 18, 2009. **Address correspondence to** B.N.; E-mail: boris.nikolic@uphs.upenn.edu

None of the authors have identified a conflict of interest.

DOI: 10.1016/j.jvir.2009.01.027

MATERIALS AND METHODS

Study Design and Animal Model

The study was performed at the animal research facility of our medical center. Approval of the institutional animal care and use committee was obtained before initiation of this study. All animals were fully anesthetized for all experiments. Anesthesia was performed via intraperitoneal injection of a mixture of 50 mg/kg body weight ketamine hydrochloride (Ketaject; Phoenix Pharmaceutical, St. Joseph, Missouri) and 5 mg/kg xylazine hydrochloride (Bayer, Shawnee Mission, Kansas). Four female Sprague-Dawley rats 6–8 weeks of age (average weight, 275 g ± 25 mg) were acquired from a single vendor (Taconic, Germantown, New York) and divided into two separate study groups with two animals in each group. All rats were subjected to intravenous administration of rat hepatic embryonic stem cells (rhESCs) that had been labeled with GFP, group I at 15 minutes after RF ablation and group II at 48 hours after RF ablation. Rats of both groups were treated equally in all study parts except for timing of rhESC administration. All animals were killed 5 days after rhESC injection. Tissue from the RF ablation area was removed, as was control tissue from nontreated hepatic parenchyma of the left hepatic lobe. The tissue samples were evaluated and compared by fluorescence microscopy for presence, extent, and distribution of rhESCs.

RF Ablation

RF ablation was performed to the right hepatic lobe at the anterior inferior portion by two operators (M.A. and P.M.) with 2 years of RF ablation operator experience in rodents. The treated location corresponded as closely as possible to human Couinaud segment V in all animals. RF ablation was performed according to a general protocol that has been described in the literature (12). Briefly, conventional monopolar RF ablation was applied in all rats with a 500-kHz RF generator (CC-1; Radionics, Burlington, Massachusetts) with a monopolar 1-cm-tip electrode (Radionics) according to a standardized protocol (mean tip temperature, 70°C ± 2°C; 140 mA ± 35, 2–5 W) for 5 minutes. The RF circuit was completed by placement of the animal on a standardized metallic grounding pad (Radionics). Findings in previous studies have shown that, with these parameters, coagulation of a 6.7-mm-diameter area can be achieved (13,14). Pad contact was ensured by shaving the animals' backs and using copious amounts of electrolytic contact gel. The tip of a 21-gauge electrically insulated electrode was placed within the right hepatic lobe under ultrasound guidance (SSD-500; 7.5-Mhz transducer; Aloka, Wallingford, Connecticut). RF ablation was applied for 5 minutes with the generator output titrated to maintain a designated tip temperature (70°C). A thermocouple at the tip of the RF electrode constantly measured the local ablation temperature, thereby enabling proper generator adjustment.

Stem Cell Infusion

All rhESCs were derived from a single cell line and purchased from the same vendor (Celprogen R, San Pedro, California). The cells were characterized by specific embryonic antigens 3 and 4, α-fetoprotein, and alkaline phosphatase as important antigenic markers, the presence of which had been verified by performance of immunocytochemistry (secondary antibody for specific embryonic antigens 3 and 4 and α-fetoprotein and primary antibody for alkaline phosphatase). Cell functionality was affirmed by performance of secondary antibody tagging for albumin (immunoglobulin G antibody conjugated with horseradish peroxidase) and enzyme-linked immunosorbent assay for transferrin identification, respectively. Cell viability of more than 99% was assured, and cell count was accomplished by the vendor through the use of Trypan blue dye in a standard hemocytometer chamber. Trypan blue dye is exclusively taken up by nonviable cells, which become identifiable with microscopic imaging.

A uniform stem cell suspension was prepared by reconstituting a 5-μL cell pellet with an additional 45 μL of 1 × phosphate buffered saline solution in a 1.6-mL Eppendorf tube. This provided a cell dilution factor of 1:10. Clumping cells were dispersed by adding 5 μl trypsin to a 50-μL cell suspension and incubating it at 37° for 15 minutes or longer, vortexing, or vigorous pipetting of the trypsin cell suspension as necessary. Subsequently, 45 μL of 0.4% Trypan blue was added to the cell suspension to enable assessment of viability and to achieve a dilution factor of 20. A cover glass was then centered over the hematocytometer chamber, both chambers were filled with 10 μL of cell/dye dilution, and the hematocytometer was placed on the microscope stage at a ×100 magnification focus. To accurately assess the viable injected cell mass, all cells (viable and nonviable) were then counted at the 1-mm center square and all four 1-mm corner squares with a hand-held counter. A recount of all five squares was then performed for all nonviable cells in the chamber (ie, blue stained cells only). This procedure was repeated for the second chamber. Adjustment for an appropriate dilution factor was performed if less than 200 or more than 500 cells were counted within the total of 10 squares. Each square of the hematocytometer represented a total volume of 0.1 mm^3, and cell count per milliliter was therefore calculated as average count per square times dilution factor × 10^4. The percentage of viable cells was calculated as the total number of viable cells divided by the total number of counted cells, and exceeded 99%.

GFP in the form of TurboGFP was used for cell labeling, which is an improved variant of the GFP CopGFP cloned from the copepod *Pontellina plumata* and reveals bright green fluorescence when expressed in eukaryotic cells (excitation wavelength, 482 nm; emission wavelength, 502 nm). Cell transfection with TurboGFP was accomplished with a lentiviral vector (Lentimax; Lentigen, Baltimore, Maryland), which was a lentivirus-based gene delivery system that was delivered into dividing and nondividing target cells' cytoplasm, where it was reverse-transcribed and integrated into the chromosomal DNA of the rhESC. Gene expression within the nucleus was mediated by a simian cytomegalovirus promoter. In vitro transfection of adherent cells was performed by Celprogen (San Pedro, California) with use of a Lentimax packaging and cell transduction system (Lentigen) per manufacturer instructions. Briefly, cells were prepared in a 24-well plate and incubated overnight at 37°C with 5% CO_2 in rhESC complete growth culture medium (Celprogen; hereon referred to as culture medium). The fol-

lowing day, 0.5 mL of nondiluted vector supernatant was diluted in culture medium and the vector and medium were mixed with gentle agitation. The culture medium was then removed and replaced by diluted vector as prepared previously and incubated at 37°C with 5% CO_2 for 6 hours along with a control sample without virus particles. The culture medium was then replaced and incubated at 37°C with 5% CO_2 for 2 days and incubated for 48 hours with culture medium. Fluorescent microscopic counting was then performed for confirmation of labeling adequacy.

Before any experiments, confocal microscopy of the delivered samples was performed at our institution to confirm proper cell labeling (**Fig 1**). GFP-labeled rhESCs were delivered in prepared syringes (1 million cells each) and suspended in 0.5 mL volume of culture medium for each injection. The cells were mixed in suspension by exposure of each syringe to a vortex shaker for 15 seconds before injection and then slowly injected into the tail vein in all animals under deep sedation.

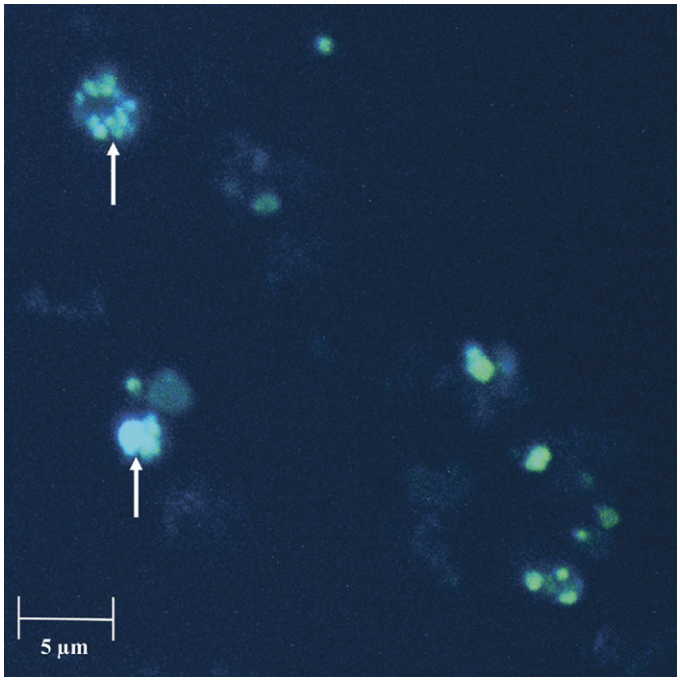

Figure 1. Confocal microscopy images of in vitro fluorescent GFP-labeled stem cells before tail vein injection. GFP causes fluorescence (straight arrows) in the cell nuclei with additional expression into the cell cytosol (no staining performed, magnification ×20, zoom ×0.7).

Tissue Processing

All four rats were euthanized with an overdose (0.2 mL/kg) of pentobarbital sodium (Nembutal; Abbott Laboratories, North Chicago, Illinois). The liver was then excised, and the ablation area in the right hepatic lobe most closely corresponding to human Couinaud segment V was identified. Similarly sized tissue blocks, approximately 9 cm^3 in volume each, were then removed with a razor blade from the RF ablation area, including the entire zone of RF ablation–induced coagulation, the periablational zone of hyperemia, and several millimeters of normal tissue peripheral to the periablational zone, as well as the left (ie, nontreated) hepatic lobe most closely corresponding to human Couinaud segment II, which served as a control in each animal. Sectioning was performed perpendicular to the path of the RF electrode. For slide preparation of liver tissue, sectioned tissue was fixed for 10 min in warm electron microscopy quality 2% paraformaldehyde/4% sucrose in Tris-buffered saline (TBS) solution and then permeabilized with 1% Triton X-100 in TBS solution for 5 minutes. The tissue blocks were then removed from TBS, blotted on filter paper to remove excess TBS, and embedded in optimal cutting temperature compound. This was followed by tissue block placement into three different changes of optimal cutting temperature compound to remove any trace of water (or TBS) and prevent ice crystals within the tissue. The tissue blocks were then placed in an optimal cutting temperature compound–filled mold and the mold held over liquid nitrogen. Within the right hepatic lobe, the RF ablation coagulation zone was easily identified macroscopically during liver section based on its appearance (pale yellow color) and textural properties that distinctly contrast with the immediately adjacent red rim reflecting periablational hyperemia and the more peripheral surrounding hepatic tissue, which remained unaffected by RF heating. For sectioning through each tissue block containing each RF ablation area, tissue block orientation was determined before subsequent slide creation at 5-μm tissue thickness. Three slides of each tissue block were generated in a way that contained part of the inner coagulation zone as well as hepatic tissue immediately adjacent and more peripheral to the area of coagulation necrosis. Hence, the orientation of the area of coagulation necrosis with respect to the immediately adjacent and more peripheral liver tissue was known for each slide before the performance of subsequent microscopy. We set aside additional corresponding tissue blocks that had not been fixed and generated slides of 10-μm tissue thickness for direct visualization of GFP by confocal microscopy (488-nm argon laser line). These were also found to be adequate for subsequent evaluation and showed results paralleling those of the samples that had been incubated with GFP antibody. Consequently, this limited the potential impact of autofluorescence in the hepatic tissues after performance of RF ablation.

Next, slide incubation in phosphate-buffered saline solution with 1% bovine serum albumin with 1:400 rabbit anti-GFP (Invitrogen, Carlsbad, California) was performed for 1 hour with gentle agitation, followed by TBS rinsing (three changes for approximately 20 minutes). The slides were then finished on slow-fade mounting media

(Invitrogen) by coverslip placement and edge enhancement with nail polish. The mounting media contained 4′,6-diamidino-2-phenylindole for cell nuclei identification to facilitate anatomic orientation. Slides were stored at −80°C.

Stem Cell Distribution Evaluation

After slide preparation from the RF-treated and control areas, the rhESC distribution pattern was assessed within the RF-treated area as well as compared between the RF ablation and the control area (ie, left hepatic lobe) in each animal. Additionally, comparisons were made between the RF ablation areas obtained from animals that had received rhESC injection 15 minutes and 48 hours after RF ablation. Evaluation was performed with a confocal microscope (LSM 510; Zeiss, Jena, Germany) that was present on site. The argon laser (458-, 477-, 488-, and 514-nm wavelengths) was used for direct GFP fluorescence visualization and the Texas red filter (HeNE; 543-nm wavelength) for GFP antibody microscopic imaging. Three separate low-power fields (×20 objective, 0.7 zoom scale magnification) of the RF ablation area were then selected in each animal in both groups. Three low-power fields of the same magnification were then randomly chosen (ie, regions first encountered during microscopy of each slide) from control tissue (ie, untreated left hepatic lobe) of each animal. Image transfer and initial processing was accomplished with LSM 510 Meta software (Zeiss). Digital images were captured from all low-power field images for subsequent biostatistical evaluation. Spatial distribution for RF ablation samples was evaluated by dividing the ablation area in three distinct zones that have been identified and described previously (15,16): zone A corresponds to the coagulation area, zone B represents the periablational margin that may be characterized by hyperemia initially and inflammatory changes several days thereafter, and zone C reflects the more peripheral hepatic parenchyma that was not subjected to substantial changes related to RF heating. The presence and extent of these zones was distinctly identified and confirmed by performance of light microscopy. Specifically, the central RF ablation area (zone A) showed nuclear deformities and clumpy cytoplasm typical of changes seen in coagulation necrosis (ie, "ghost appearance"). The immediate adjacent hepatic parenchyma represents zone B and is characterized by intense stem cell uptake in our experimental study, such that the transition between zone A and zone B could be distinctly identified microscopically. The more peripheral hepatic parenchyma that neighbors zone B constitutes zone C and did not show any changes characteristic of coagulation necrosis whatsoever.

Table 1
Comparison of Stem Cell Distribution in Each Animal

Measurement	Stem Cell Count*	
	RF Ablation Area	Corresponding Control Tissue
Injection 15 min after RF ablation		
Median	9,847.5	1,335
Mean ± SD	10,471 ± 3,830	1,889 ± 1,427
Injection 48 h after RF ablation		
Median	14,024.5	3,313.5
Mean ± SD	15,177 ± 7,091	2,868 ± 1,714

* Fluorescent pixel count reflecting stem cell uptake.

Image Evaluation

Quantitative distribution was evaluated by performance of GFP antibody fluorescent counts of each captured digital image with use of the ImageJ software package (National Institutes of Health, Bethesda, Maryland). This software enables the user to choose a defined constant threshold of pixel brightness, which allowed us to select and count all pixels reflecting GFP antibody fluorescence. Fluorescence originating from 4′,6-diamidino-2-phenylindole staining was excluded from analysis. Fluorescence counts were obtained for each digital image of each RF ablation zone and each digital image from corresponding control tissue of each animal (Table 1). Fluorescence counts of each RF ablation area reflected collective measurements of equal-sized areas of coagulation necrosis and periablational and more peripheral zones for comparative analysis versus control tissue. Evaluation of zonal rhESC distribution within the RF ablation areas (ie, zone A corresponds to coagulation area, zone B represents the periablational margin, and zone C reflects the more peripheral normal-appearing hepatic parenchyma) was performed by two separate, defined, and equal-sized high-power field sample areas of each zone (ie, regions of interest), which were selected from opposite halves of each slide (ie, top and bottom or left and right) and viewed as high-power field images at ×10 magnification (Fig 2). Fluorescent count of these extracted sample areas of each zone was performed with use of ImageJ software, as described earlier, and the mean of both selected sample areas for each zone was calculated.

Statistical Analysis

All fluorescent counts were entered into an Excel spreadsheet (Microsoft, Redmond, Washington). Study group results were compared with those from the respective control samples with a nonparametric Kruskal-Wallis test. Comparisons between the results for each zone were likewise performed by nonparametric Kruskal-Wallis analysis. The animals that received rhESC injection 15 minutes after RF ablation (group I) were additionally compared with those that received rhESC injection 48 hours after RF ablation (group II). For all comparisons, a P value less than .05 was considered significant.

RESULTS

The mean fluorescent count in the animals that had received rhESC injection 15 minutes after RF ablation (study group I) was 10,471 ± 3,830

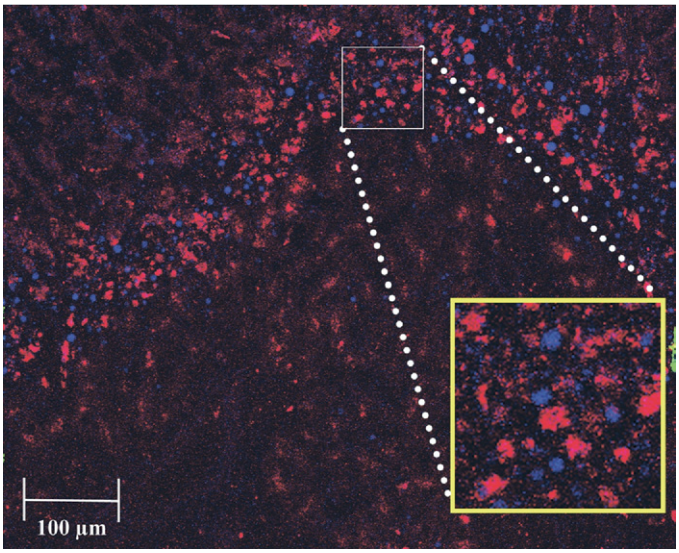

Figure 2. Schematic example of selection of defined sample area (ie, region of interest) for each zone (white/yellow square). Two of these areas were selected from each zone, 10 × magnified, and submitted for fluorescence count analysis.

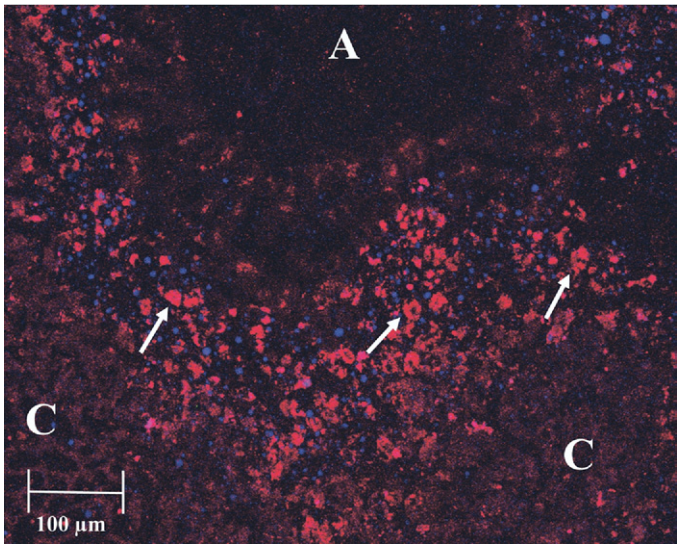

Figure 3. Antibody-stained fluorescent images after RF ablation (magnification 20, zoom ×0.7) show stem cell uptake at coagulation margin with fluorescent stem cells (arrows), coagulation area (A) and the more peripheral hepatic parenchyma not subjected to substantial changes from RF ablation heating (C). Focal blue areas of fluorescence represent 4′,6-diamidino-2-phenylindole stain of nuclei as anatomic markers and are unrelated to stem cell labelling.

(SD; median, 9,847.5), compared with a mean count of 1,889 ± 1,427 (median 1,335) for the corresponding control tissue from the same animals ($P < .05$; **Figs 3,4**; **Table 1**). The mean fluorescent count of the animals that underwent rhESC injection 48 hours after RF ablation (study group II) was 15,177 ± 7,091 (median, 14,024.5), compared with a mean count of 2,868 ± 1,714 (median, 3,313.5) in the corresponding control group ($P < .05$; **Table 1**).

Analysis for stem cell uptake between RF ablation zones had absolute fluorescent counts that were substantially lower for these sample areas than for the lower-power, more global images that had been used for the initial comparative analysis between the RF ablation territories and corresponding control tissue for each animal, as these sample regions of interest represented only small magnified parts of each zone that had been extracted from the initial more global image of the RF ablation area (**Fig 2**). Stem cells were concentrated at the periablational area in all animals, and the variation of fluorescent counts across zonal distribution among all animals was significant ($P < .05$; zone B, mean, 1,015.4 ± 311 [median, 874.5]; zone A, mean, 17.8 ± 11 [median, 16]; zone C, mean, 141.2 ± 51.4 [median, 138]; **Figs 2,3,5**; **Table 2**). No substantial difference in fluorescence counts was found between animals that received rhESCs 15 minutes versus 48 hours after RF ablation; no statistics were analyzed given the lack of a substantial trend in pixel count difference between study groups and the small size of each group.

DISCUSSION

Our results confirmed the hypothesis that stem cells injected after the performance of RF ablation are directed in significantly higher numbers to the periablational margin surrounding the coagulation zone induced by RF ablation than to the remaining liver. Histologic analysis of the RF ablation area shows three distinct zones: zone A represents the central area of coagulation necrosis, zone B reflects a distinct tissue rim around the immediate area of coagulation necrosis, and zone C constitutes hepatic parenchyma that is peripheral to zone B. Stem cell uptake is significantly higher at the periablational tissue rim (ie, zone B) than the adjacent more peripheral hepatic parenchyma (ie, zone C), into which focal stem cell extension occasionally occurs. The coagulation area (ie, zone A) is largely devoid of stem cell uptake, likely because the blood flow needed for stem cell delivery is absent in this area of necrosis.

We propose two possibly synergistic mechanisms that may cause the stem cell distribution pattern that was found in our study. First, stem cell trafficking to the area of acute organ injury has been linked to the release of certain key cytokines and other factors, such as interleukin 6, vascular endothelial growth factor, and hepatocyte growth factor; this has also been shown to be associated with increasing serum blood levels after the performance of RF ablation (8,11). Acute injury–related release of certain key cytokines and proteins therefore likely largely contributes to stem cell trafficking to the area of RF ablation. However, we also theorize that increased blood flow in the periablational zone caused by postablation hyperemia may additionally impact stem cell distribution, as high periablational (ie, zone B) concentrations were previously found in the setting of intravenous liposomal doxorubicin administration as well (15). Although stem cell trafficking through cytokine-mediated chemoattraction has been identified and reported in the literature, the stem cell distribution that was found in our study is the result of a novel concept of stem cell administration after performance of RF ablation (17,18). Hence, stem cell distribution patterns as a consequence of permeability effects resulting from energy deposi-

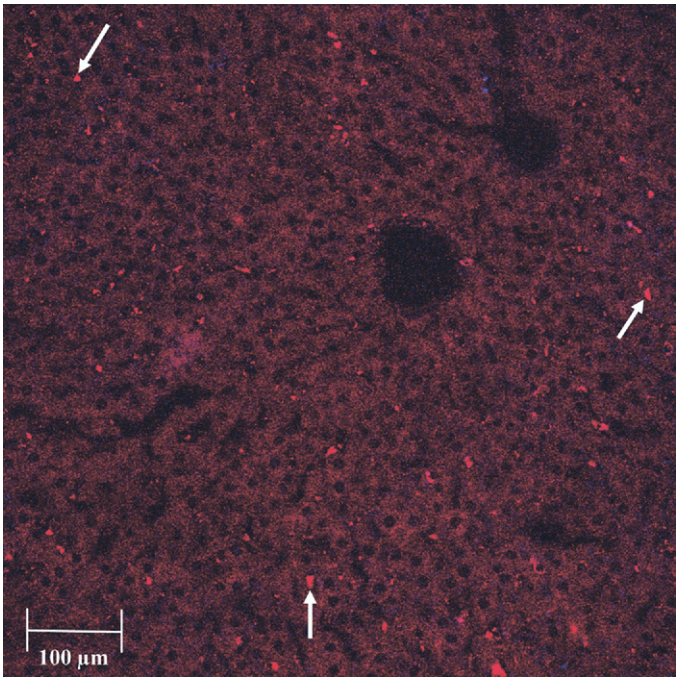

Figure 4. Typical examples of hepatic control tissue obtained from the same animal as **Figures 3 and 4** (magnification ×20 objective, zoom ×0.7): fluorescent stem cells (straight arrows) are identified in a random pattern and much less concentrated than around the area of RF ablation (compare with **Figs 3,4**). Focal blue areas of fluorescence represent 4′,6-diamidino-2-phenylindole stain of nuclei as anatomic markers and are unrelated to stem cell labeling.

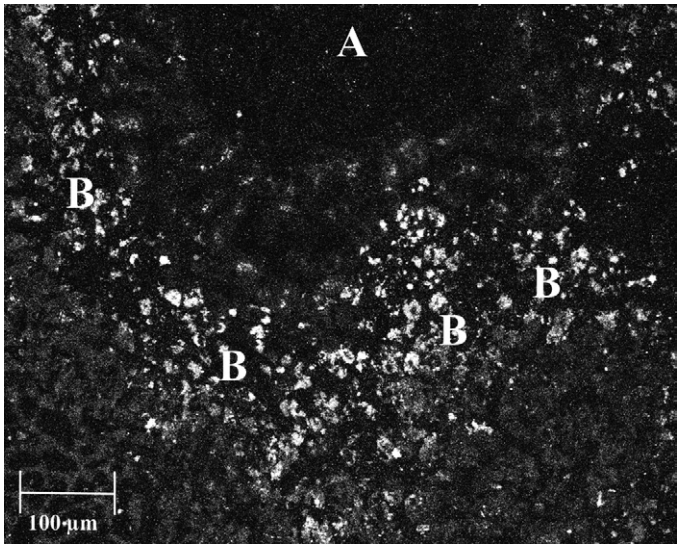

Figure 5. Gray scale image obtained from light microscopy showing zonal distribution: Coagulation necrosis: zone A (A), periablational area exhibiting maximal stem cell uptake: zone B (B) and more peripheral hepatic parenchyma: zone C (C).

tion as opposed to biologic effect (eg, active chemotactic cell recruitment) must be considered, and clarification will be provided through future experimental investigation. In addition, it appears that the exact mechanisms of stem cell trafficking and cell interaction warrant further specification through future research.

In this study, we injected stem cells at two different time points (15 minutes and 48 hours) after the performance of RF ablation. These time points were chosen because the composition of the periablational zone changes over time: initial hyperemia is replaced by an influx of inflammatory cells, with the presence of macrophages and giant cells noted several days after ablation, which was assumed to impact stem cell trafficking secondary to changes in blood flow patterns in the periablational area. Even though we did not find stem cell distribution to be substantially different between these two groups, it is likely that stem cell injection at various additional time points nevertheless will influence stem cell trafficking to the ablation area. However, relevance of stem cell administration timing is likely mostly determined by peak release of certain key cytokines at specific time points that actively direct stem cells, rather than just to the occurrence of changes in blood flow patterns in the periablational area resulting in passive increased uptake. Specifically, Evrard et al (11) found a peak increase of interleukin 6 levels at 3 hours, a threefold maximum increase of hepatocyte growth factor on day 1, and an increase of vascular endothelial growth factor commencing on day 5 after the performance of RF ablation.

In previous animals models, hepatic injury had been inflicted by performance of partial hepatectomy or hepatic injection of carbon tetrachloride (7,9,10). These experiments had shown the ability of stem cells to engraft to fully functional parenchymal cells in the appropriate microenvironment (7,9,10). In a more recent clinical study (19), hepatic regeneration could be enhanced by portal venous infusion of bone marrow–derived stem cells into portal vein branches before portal vein embolization and performance of partial hepatectomy. Unlike with performance of partial hepatectomy, RF ablation does not result in excision of hepatic tissue but is applied in a way that creates a coagulation zone that may trigger stem cell trafficking and migration, along with ingrowth of granulation tissue over a period of time. Indeed, the capacity of stem cells to migrate has been demonstrated for oligodendrocyte progenitor cells as well as for embryonic stem cells after stroke induction in the rat model (20,21). Expansion of the follow-up time frame will therefore be necessary to evaluate for potential stem cell migration and population of the coagulation area over time. Accordingly, we hypothesize that the coagulation area that is created by RF ablation represents potential additional engraftment territory, which, if verified in the future, could be a significant advantage of RF ablation versus partial hepatectomy or the poorly controllable intrahepatic injections of toxic liquids, both of which generally limit stem cell transplantation to the size of the (sub-

Table 2
Zonal Analysis of Stem Cell Distribution of RF Ablation Areas in All Animals

	Stem Cell Count*		
Measurement	Zone A	Zone B	Zone C
Median	16	874.5	138
Mean ± SD	17.8 ± 11	1,015.4 ± 311	141.2 ± 51.4

* Fluorescent pixel count reflecting stem cell uptake.

endothelial) space of Disse of the recipient liver (22).

Additionally, RF ablation can be performed sequentially in different anatomic areas of the liver over time and is fairly well tolerated, spatially quite precise, and clinically well established. Consequently, large volumes of a target organ such as the liver could be treated over a period of time for the purpose of therapeutic tissue conversion, ie, the simultaneous removal of malignant or dysfunctional tissue and facilitation of subsequent tissue reengineering through stem cell differentiation into fully functional parenchymal cells in the same anatomic area. Hence, substantial and sufficient portions of the liver could potentially be subjected to RF ablation–induced tissue engineering, resulting in significant improvement of organ function. Indeed, although RF ablation of a region of the liver alone is unlikely to improve liver regeneration in humans, it nevertheless is likely to provide an excellent adjunctive strategy for promoting such regeneration by dramatically improving trafficking of the very stem cells that can achieve this purpose.

Although the presented experimental concept thus holds promise for the future, it constitutes a pilot project and was designed to investigate the potential of RF ablation as a vehicle for stem cell trafficking to the liver. We acknowledge that our study represents only the initial step in the evaluation of RF ablation as a tool for tissue conversion. We are therefore currently preparing more systematic investigations to determine whether stem cells injected after the performance of RF ablation will differentiate into fully functional hepatocytes over time. This evaluation requires longer-term follow-up and performance of subsequent immunofluorescent staining for hepatocytic markers such as α-fetoprotein, cytokeratin-19, and albumin at various follow-up time points after stem cell injection, and was beyond the scope of this initial feasibility study (23). In addition, we will evaluate whether stem cell engraftment after the performance of RF ablation is sustainable over time. Demonstration of sustainable stem cell engraftment facilitated through the performance of RF ablation could be of clinical potential in patients with benign chronic liver disease, such as liver cirrhosis and metabolic liver disease. In addition, further study of this concept in the setting of hepatic malignancy may be considered because RF ablation is routinely used clinically for locoregional tumor therapy. Particularly in the setting of hepatocellular carcinoma, functional liver reserve is often decreased and may deteriorate further with performance of locoregional therapy (24). However, stem cell administration after RF ablation treatment for malignancy likewise mandates careful long-term follow-up given the theoretically implied risk of cell fusion and potential unwarranted cell therapy–based tumor propagation, and this type of evaluation was not part of the objective of this feasibility study.

Nevertheless, all these categories of patients could potentially greatly benefit from replacement of the RF-ablated area by stem cell–engineered, fully functional parenchyma.

Instead of using stem cells of embryonic origin as in this study, skin- and bone marrow–derived stem cells should also be assessed in the future, as these have the potential benefit of being able to be harvested as autologous cells. If these cell lines can be successfully engrafted for the purpose of tissue conversion, translation of our technique to a clinical application in the future would be more readily conceivable.

An additional paradigm likely worthy of serious consideration is the evaluation whether targeted delivery, particularly transarterial delivery of stem cells, may be more efficient than random—ie, peripheral venous—delivery of stem cells. Transarterial stem cell administration may increase targeted delivery efficiency if performed at a time of rich granulation tissue formation and/or maximum release of certain key cytokines. A "preformed vascular bed" has previously been postulated to additionally facilitate stem cell engraftment—at least in the context of myocardial tissue engineering—and would likely most efficiently be reached by transarterial cell delivery (25).

Additional experiments are necessary and currently under way to optimize stem cell trafficking to the RF ablation area, as well as to demonstrate full and sustainable stem cell engraftment after the performance of RF ablation.

Limitations of the current study include its pilot character, which does not allow for general conclusions with regard to the utility of RF ablation as a tool for sustainable long-term reengineering of hepatic (or other) parenchyma. We acknowledge that, despite the fact that the results were highly significant between the study and corresponding control samples, only two animals were included in each group. Nevertheless, as described earlier, the promising data gleaned from this study clearly point to the next steps for future proposed research.

In summary, stem cells administered after RF ablation are trafficked to the peri-ablational tissue in significantly higher numbers than to the remaining liver. Hence, RF ablation may become a useful tool to promote stem cell engraftment.

Acknowledgment: This work was supported in part by an institutional seed grant from the Department of Radiology at Beth Israel Deaconess Medical Center (Boston, Massachusetts). The authors also acknowledge Esmail Zanjani, ED, PhD, Graca Almeida-Porada, MD, PhD, and Harold Brodofel, MD.

References

1. Lagasse E, Connors H, Al-Dhalimy M, et al. Purified hematopoietic stem

cells can differentiate into hepatocytes in vivo. Nat Med 2000; 6:1229–1234.
2. Takahashi M, Nakamura T, Toba T, Kajiwara N, Kato H, Shimizu Y. Transplantation of endothelial progenitor cells into the lung to alleviate pulmonary hypertension in dogs. Tissue Eng 2004; 10:771–779.
3. Heine W, Conant K, Griffin JW, Hoke A. Transplanted neural stem cells promote axonal regeneration through chronically denervated peripheral nerves. Exp Neurol 2004; 189:231–240.
4. Bos C, Delmas Y, Desmouliere A, et al. In vivo MR imaging of intravascularly injected magnetically labeled mesenchymal stem cells in rat kidney and liver. Radiology 2004; 233:781–789.
5. Hauger O, Frost EE, van Heeswijk R, et al. MR evaluation of the glomerular homing of magnetically labeled mesenchymal stem cells in a rat model of nephropathy. Radiology 2006; 238:200–210.
6. Sutton EJ, Henning TD, Pichler BJ, Bremer C, Daldrup-Link HE. Cell tracking with optical imaging. Eur Radiol 2008.
7. Yin Y, Lim YK, Salto-Tellez M, Ng SC, Lin CS, Lim SK. AFP(+), ESC-derived cells engraft and differentiate into hepatocytes in vivo. Stem Cells 2002; 20:338–346.
8. Dalakas E, Newsome PN, Harrison DJ, Plevris JN. Hematopoietic stem cell trafficking in liver injury. FASEB J 2005; 19:1225–1231.
9. Yamamoto H, Quinn G, Asari A, et al. Differentiation of embryonic stem cells into hepatocytes: biological functions and therapeutic application. Hepatology 2003; 37:983–993.
10. Kobayashi N, Ando M, Kosaka Y, et al. Partial hepatectomy and subsequent radiation facilitates engraftment of mouse embryonic stem cells in the liver. Transplant Proc 2004; 36:2352–2354.
11. Evrard S, Menetrier-Caux C, Biota C, et al. Cytokines pattern after surgical radiofrequency ablation of liver colorectal metastases. Gastroenterol Clin Biol 2007; 31:141–145.
12. Mertyna P, Hines-Peralta A, Liu ZJ, Halpern E, Goldberg W, Goldberg SN. Radiofrequency ablation: variability in heat sensitivity in tumors and tissues. J Vasc Interv Radiol 2007; 18:647–654.
13. Goldberg SN, Kruskal JB, Oliver BS, Clouse ME, Gazelle GS. Percutaneous tumor ablation: increased coagulation by combining radio-frequency ablation and ethanol instillation in a rat breast tumor model. Radiology 2000; 217:827–831.
14. Goldberg SN, Saldinger PF, Gazelle GS, et al. Percutaneous tumor ablation: increased necrosis with combined radio-frequency ablation and intratumoral doxorubicin injection in a rat breast tumor model. Radiology 2001; 220:420–427.
15. Monsky WL, Kruskal JB, Lukyanov AN, et al. Radio-frequency ablation increases intratumoral liposomal doxorubicin accumulation in a rat breast tumor model. Radiology 2002; 224:823–829.
16. Ahmed M, Lukyanov AN, Torchilin V, Tournier H, Schneider AN, Goldberg SN. Combined radiofrequency ablation and adjuvant liposomal chemotherapy: effect of chemotherapeutic agent, nanoparticle size, and circulation time. J Vasc Interv Radiol 2005; 16:1365–1371.
17. Bird TG, Lorenzini S, Forbes SJ. Activation of stem cells in hepatic diseases. Cell Tissue Res 2008; 331:283–300.
18. Laird DJ, von Andrian UH, Wagers AJ. Stem cell trafficking in tissue development, growth, and disease. Cell 2008; 132:612–630.
19. Furst G, Schulte am Esch J, Poll LW, et al. Portal vein embolization and autologous CD133+ bone marrow stem cells for liver regeneration: initial experience. Radiology 2007; 243:171–179.
20. Bulte JW, Zhang S, van Gelderen P, et al. Neurotransplantation of magnetically labeled oligodendrocyte progenitors: magnetic resonance tracking of cell migration and myelination. Proc Natl Acad Sci U S A 1999; 96:15256–15261.
21. Hoehn M, Kustermann E, Blunk J, et al. Monitoring of implanted stem cell migration in vivo: a highly resolved in vivo magnetic resonance imaging investigation of experimental stroke in rat. Proc Natl Acad Sci U S A 2002; 99:16267–16272.
22. Gupta S, Rajvanshi P, Lee CD. Integration of transplanted hepatocytes into host liver plates demonstrated with dipeptidyl peptidase IV-deficient rats. Proc Natl Acad Sci U S A 1995; 92:5860–5864.
23. Nonome K, Li XK, Takahara T, et al. Human umbilical cord blood-derived cells differentiate into hepatocyte-like cells in the Fas-mediated liver injury model. Am J Physiol Gastrointest Liver Physiol 2005; 289:G1091–G1099.
24. Huo TI, Lee PC, Huang YH, et al. The sequential changes of the model for end-stage liver disease score correlate with the severity of liver cirrhosis in patients with hepatocellular carcinoma undergoing locoregional therapy. J Clin Gastroenterol 2006; 40: 543–550.
25. Naito H, Melnychenko I, Didie M, et al. Optimizing engineered heart tissue for therapeutic applications as surrogate heart muscle. Circulation 2006; 114: I72–I78.